

Article

Effect of Graphene Additive on Flexural and Interlaminar Shear Strength Properties of Carbon Fiber-Reinforced Polymer Composite

Mohamed Ali Charfi ¹, Ronan Mathieu ¹, Jean-François Chatelain ^{1,*},
Claudiane Ouellet-Plamondon ²  and Gilbert Lebrun ³

¹ École de Technologie Supérieure, Mechanical Engineering Department, Montréal, QC H3C1K3, Canada; mohamed-ali.charfi.1@ens.etsmtl.ca (M.A.C.); ronan.mathieu.1@ens.etsmtl.ca (R.M.)

² École de Technologie Supérieure, Construction Engineering Department, Montréal, QC H3C1K3, Canada; claudiane.ouellet-plamondon@etsmtl.ca

³ Mechanical Engineering Department, Université du Québec à Trois-Rivières (UQTR), Trois-Rivières, QC G8Z 4M3, Canada; gilbert.lebrun@uqtr.ca

* Correspondence: jean-francois.chatelain@etsmtl.ca; Tel.: +1-514-396-8512

Received: 28 September 2020; Accepted: 26 October 2020; Published: 30 October 2020



Abstract: Composite materials are widely used in various manufacturing fields from aeronautic and aerospace industries to the automotive industry. This is due to their outstanding mechanical properties with respect to their light weight. However, some studies showed that the major flaws of these materials are located at the fiber/matrix interface. Therefore, enhancing matrix adhesion properties could significantly improve the overall material characteristics. This study aims to analyze the effect of graphene particles on the adhesion properties of carbon fiber-reinforced polymer (CFRP) through interlaminar shear strength (ILSS) and flexural testing. Seven modified epoxy resins were prepared with different graphene contents. The CFRP laminates were next manufactured using a method that guarantees a repeatable and consistent fiber volume fraction with a low porosity level. Short beam shear and flexural tests were performed to compare the effect of graphene on the mechanical properties of the different laminates. It was found that 0.25 wt.% of graphene filler enhanced the flexural strength by 5%, whilst the higher concentrations (2 and 3 wt.%) decreased the flexural strength by about 7%. Regarding the ILSS, samples with low concentrations (0.25 and 0.5 wt.%) demonstrated a decent increase. Meanwhile, 3 wt.% slightly decreases the ILSS.

Keywords: CFRP; composite; graphene; contact molding; mechanical properties

1. Introduction

Carbon fiber-reinforced polymer composites (CFRP) are increasingly being used in a wide range of domestic and industrial applications, such as aerospace, automobile, wind energy, sport, and goods industries, to name a few [1,2]. Owing to their advantageous properties like corrosion resistance, temperature resistance, light weight, and high mechanical properties, more than 50% of new aircrafts (Airbus A350 and Boeing 787) are composed of CFRP [3,4]. Their strength/weight and stiffness/weight ratios can be five to eight times greater than ordinary metals [5]. However, the matrix/fiber interface is considered as the weakest link of composite materials [6], with typical flaws such as voids and uncovered fibers. This would eventually initiate the failure of composite parts [7].

As a solution for interfacial weaknesses, researchers have sought to incorporate fillers in the matrix. These fillers have great potential to ameliorate the mechanical, chemical, and physical properties of the polymer. Therefore, enhancing the matrix bonding properties should improve the overall composite quality [8,9]. Graphene is one of the most promising fillers in polymers. Since its first discovery in

2004 [10], this material has gained enormous attention [11,12]. It possesses exceptional characteristics like high thermal and electrical conductivity [13,14] and being lightweight, as well as astonishing mechanical properties [15,16]. Graphene is usually obtained through the exfoliation of graphite. However, its manufacturing is cost-prohibitive and presents safety risks in large-scale production [17]. Graphene materials are good fillers for polymer matrices, with nano-clay and carbon nanotubes being the most relevant competitors. Both graphene and nano-clay are platelet-type materials, characterized by a layered structure with high aspect ratios (>1000) [18,19]. Composite polymers based on platelet fillers demonstrated outstanding mechanical properties. However, graphene outperforms nano-clay by its excellent thermal and electrical properties. In contrast, carbon nanotubes possess similar thermal and electrical properties to graphene. However, they are not considered as suitable fillers because of their relatively expensive, high mixture viscosity causing the entangling of nanotubes, and immense anisotropic properties [20]. Another comparative study [21] was performed between graphene nano-platelets (GnPs), single-walled carbon nanotubes (SWCNT), and multi-walled carbon nanotubes (MWCNT). The Young's modulus of the graphene nanocomposite is 31% higher than that of the pristine epoxy as opposed to only 3% enhancement for the SWCNT. Moreover, the tensile strength of the graphene nanocomposite is 26% higher than that based on MWCNT [21]. This renders graphene nanoplatelets the ideal filler for our experiments. Homogeneous dispersion, graphene exfoliation, and load percentage play a vital role in the composite quality. For instance, while flexural stress and short beam shear stress tend to peak at lower graphene percentages, electrical and thermal conductivity significantly increase at higher filler percentages. Moreover, dispersion and exfoliation processes have an undeniable impact on the composite quality [22].

Han et al. [23] studied the impact of graphene oxide (GO) concentration on the interlaminar shear strength (ILSS) of CFRP laminates. From 0 to 0.1 wt.%, the ILSS increased but beyond 0.2 wt.%, the ILSS was inversely proportional to the GO content. Indeed, a maximum improvement of more than 8% was recorded at 0.1 wt.% compared to the same composite without graphene. The same tendency was observed by Kamar et al. [24], who used glass fabric composites with GnPs particles. The optimum graphene concentration was 0.25 wt.%, which induced 29% and 25% of improvement in flexural strength and mode I fracture toughness, respectively. Increasing the concentration to more than 0.5 wt.% considerably reduces the fracture toughness and decreases the interlaminar adhesion which in turn leads to delamination and micro-buckling.

Tang et al. [25] investigated the influence of graphene dispersion in epoxy. They prepared two graphene/epoxy mixtures with 0.2 wt.% by means of the ball mill mixing technique. The graphene particles were better dispersed in one mixture than the other. As a result, highly dispersed graphene induces higher strength and fracture toughness. The fracture improvement was 52% for the highly-dispersed mixture as opposed to only 24% for the poorly dispersed mixture. A similar study conducted by Raza et al. [26] concluded that graphene dispersed by mechanical mixing produces better thermal and electrical conductivity than when prepared by a dual asymmetric centrifuge speed mixer. This trend is attributed to the intensive shearing of mechanical mixing. Chandrasekaran et al. [27] compared the electrical properties of two different processing methods: the high-shear mixing plus three-roll milling method (3RM) against the high-shear mixing plus sonication method, emphasizing that samples prepared by 3RM have a higher electrical conductivity than those prepared by sonication.

The fiber volume fraction variation (V_f) and porosity contents are crucial factors to drive a clear conclusion of this study. The composite properties are dominated by the fiber properties and not by the matrix (i.e., Young's modulus, flexural strength, etc.) [28]. Thereby, any trivial variation of the fiber volume fraction would conceal the impact of graphene. Similarly, the void ratio negatively affects the properties. For example, interlaminar shear strength decreases by about 7% per 1% of void content [29]. Therefore, all samples must have the same V_f with a minimum of variation as well as low and consistent porosity.

To the best of the authors' knowledge, most of the manufactured laminates presented by previous studies possess either a relatively large V_f variation or a non-uniform filler dispersion which might

affect the repeatability of their results. For example, in [24,30,31], the authors incorporated different types of particles into the laminate by means of vacuum resin transfer molding (VARTM). Even though this technique might lead to a consistent fiber volume fraction, it may lead to non-uniform dispersion of the filler particles because of a “filtering” mechanism of the filler by the fibers all along the resin transfer. Mclaughlin [28] used hand-layup and vacuum bagging with weight control of the fibers and the epoxy. Nevertheless, the fiber volume fraction was not found repeatable from one laminate to another. For these reasons, the first objective of this study is to propose an innovative and reliable manufacturing method, at a reasonable cost for experiment purposes, that leads to clear conclusions about the effect of graphene on the mechanical properties. It is important to note that this study is a part of a larger scientific study, with the main goal of improving the machinability of CFRP. This material is inherently rough and abrasive which makes its machinability more difficult than other materials. Tool wear and poor surface finish frequently occur in this matter [31]. So, enhancing the machinability of CFRP is a necessity. However, we still have to improve or, at least maintain, the mechanical properties of the modified material as compared to the unfilled resin composite. We also investigate the optimum filler percentage that induces the best short beam shear (SBS) and flexural strengths. The results found of this study are the starting point to find the best filler percentage that improves the machinability of CFRP.

2. Materials and Methods

In this section, we present the samples preparation in four principle paragraphs: the graphene/epoxy mixing process, the CFRP laminate manufacturing method, composite quality verification, and the mechanical tests. Concerning the quality verification, this was carried out by analyzing the fiber volume fraction and the porosity content. The mechanical properties were evaluated through SBS and flexural tests. Both SBS and flexural coupons possess a rectangular shape. However, SBS is smaller than the flexural coupon, with a length and a width of only 18 and 8 mm, respectively.

2.1. Graphene-Epoxy Mixing Process

Graphene particles (0XB) were provided by Nano-Xplore Inc. (Saint-Laurent, QC, Canada). These particles were mixed and exfoliated within a Marine 820 epoxy resin from Axson Technologies (Madison Heights, MI, USA). The filler percentages varied from 0 to 3 wt.%, as presented in Table 1.

Table 1. Graphene’s percentages.

Test Number	Graphene (wt. %)
1	0
2	0.25
3	0.50
4	0.75
5	1.00
6	2.00
7	3.00

Filler percentages were calculated with respect to the total weight of the mixture which includes the hardener weight, epoxy weight, and filler weight. According to the epoxy supplier, the weight ratio of hardener/epoxy should be 18%. The following equations present the weight of each part of the mixture.

$$W_h = 0.18 \times W_{ep} \tag{1}$$

$$W_g = \text{wt.}\% \times W_t \tag{2}$$

$$W_t = W_{ep} + W_h + W_g \tag{3}$$

$$W_g = (\text{wt.}\% \times 1.18W_{ep}) / (1 - \text{wt.}\%) \tag{4}$$

Here, W_h is the hardener weight (g); W_g is the graphene weight percentage (g); W_{ep} is the epoxy weight (g), and W_t is the total weight (g).

Based on previous studies [23,24], we used three-roll milling (3RM) and high-shear mixing to incorporate and homogenize graphene particles in the epoxy. Next, a Silverson L5M-A (Silverson Machines, Inc., East Longmeadow, MA, USA) high-shear mixer was used to mechanically blend the filled epoxy. The intensive shear force deeply exfoliates the graphene particles which considerably reduces the flakes' thickness. As shown in Table 2, the mechanical mixing was divided into seven segments, during which the temperature was almost maintained with the help of an ice bath. However, the ice bath was removed in the last step to allow the temperature to rise to a maximum of 50 °C. The elevated temperature decreased the mixture viscosity, facilitating air bubble extraction. [31].

Table 2. Shear mixing sequence.

Time	Speed (RPM)
2 min	1000
2 min	3500
2 min	6000
2 min	8000
2 × 3 min	10,000

Final degassing was done in a vacuum oven for one hour, and the loaded epoxy was finally mixed with the hardener according to the supplier's instructions.

2.2. Laminate Manufacturing

The following constraints are imposed on the manufacturing method in this study: homogeneous distribution of graphene, consistent laminate thickness, minimum void, and minimum fluctuation of the fiber orientation. Even though there are multiple processing methods, most of them are either expensive or difficult to operate and unadjustable to meet the above-mentioned requirements, especially the one requiring a homogeneous distribution of filler particles. In this context, contact molding was the only alternative to liquid injection molding processes for this scientific application. Since the operator impregnates the fiber layer by layer with the filled epoxy, the graphene particles are evenly dispersed on the surface of each layer as well as across the laminate thickness. Nonetheless, the basic contact molding process usually produces important void contents, stochastic fiber angle fluctuation, and uncontrollable thickness variations. The void ratio can be reduced by applying a vacuum during the cure of the plate to remove most of the trapped air from the laminate [32]. In terms of angle fluctuations of the fiber, three wooden sticks with several grooves were fixed on top of the mold (Figure 1). These sticks form a frame that prevents the fiber layers from slipping during the hand-layup and the curing processes. These grooves allow the excess of epoxy to be expelled without displacing the wooden sticks.



Figure 1. Guide frame wooden stick.

A uniform laminate thickness was obtained using four spacers having the same thickness. These spacers were placed on the mold, distanced from the wooden frame by approximately 10 mm on each side. This technique improved the hand-layup process and made it adequate for this study. Figure 2 presents a 3D sketch of the developed method.

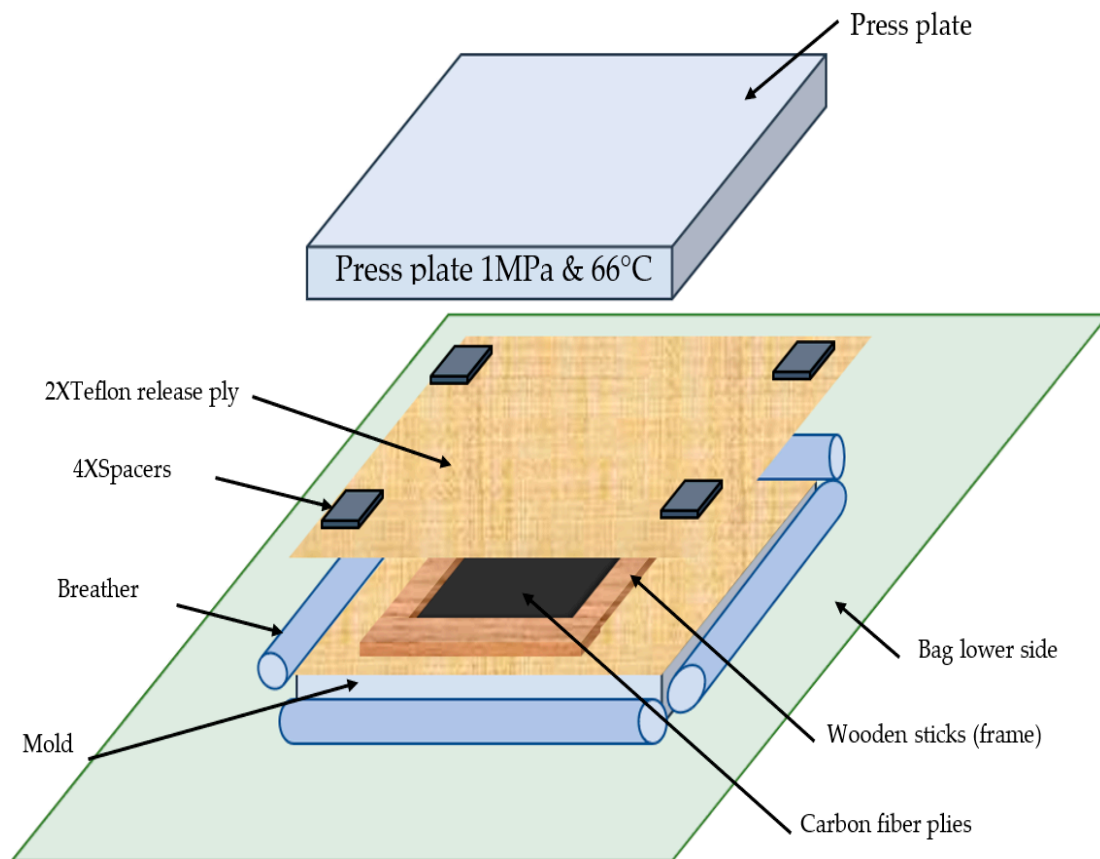


Figure 2. Exploded view of the layup assembly.

Fourteen plies of TC-09-U unidirectional high-modulus carbon fiber from Texonic Inc. (Saint-Jean-sur-Richelieu, QC, Canada) were used to form $[0]_{14}$ laminates with a thickness of around 4 mm. The single-layer reinforcement surface density is 320 g/m^2 . In terms of curing parameters, the vacuum pressure was set at a maximum of 29 inches of mercury, and the hydraulic press was equipped with heater plates which allow for curing the laminate according to the supplier recommendation, at $66 \text{ }^\circ\text{C}$ for 3 h and under a pressure of 1 MPa to have a consistent thickness. Figure 3 shows a typical photograph of the developed method. As for the demolding part, we used a Teflon sheet instead of a release agent and peel ply. Indeed, the release agent was not effective under such curing conditions. In addition, the peel ply randomly absorbs a certain quantity of epoxy which affects the fiber volume fraction. Conversely, the Teflon sheet is quite efficient during the demolding and its intrinsic sealant nature guarantees a smooth surface on both sides of the plaque.

A post-curing was required to uniformize curing through the thickness of the laminates. Therefore, all the plates were put inside a Despatch oven (Ontario Ovens Inc., Brampton, ON, Canada) which was programmed to gradually increase the temperature with a segment ramp of $10 \text{ }^\circ\text{C}$ per hour until it reaches a maximum of $66 \text{ }^\circ\text{C}$. The temperature was held constant for 24 h. Eventually, it gradually decreases with a negative slope of $10 \text{ }^\circ\text{C}$ per hour until reaching room temperature. Verification of the laminate quality was performed through measurement of the fiber volume fraction (V_f) and void ratio. To avoid oxidation of carbon fibers using a high temperature of pyrolysis when measuring V_f [29,30], it was instead calculated by measuring the laminate thickness and implementing it into Equation (5).

$$V_f = (M_f \times N) / (\rho \times h) \quad (5)$$

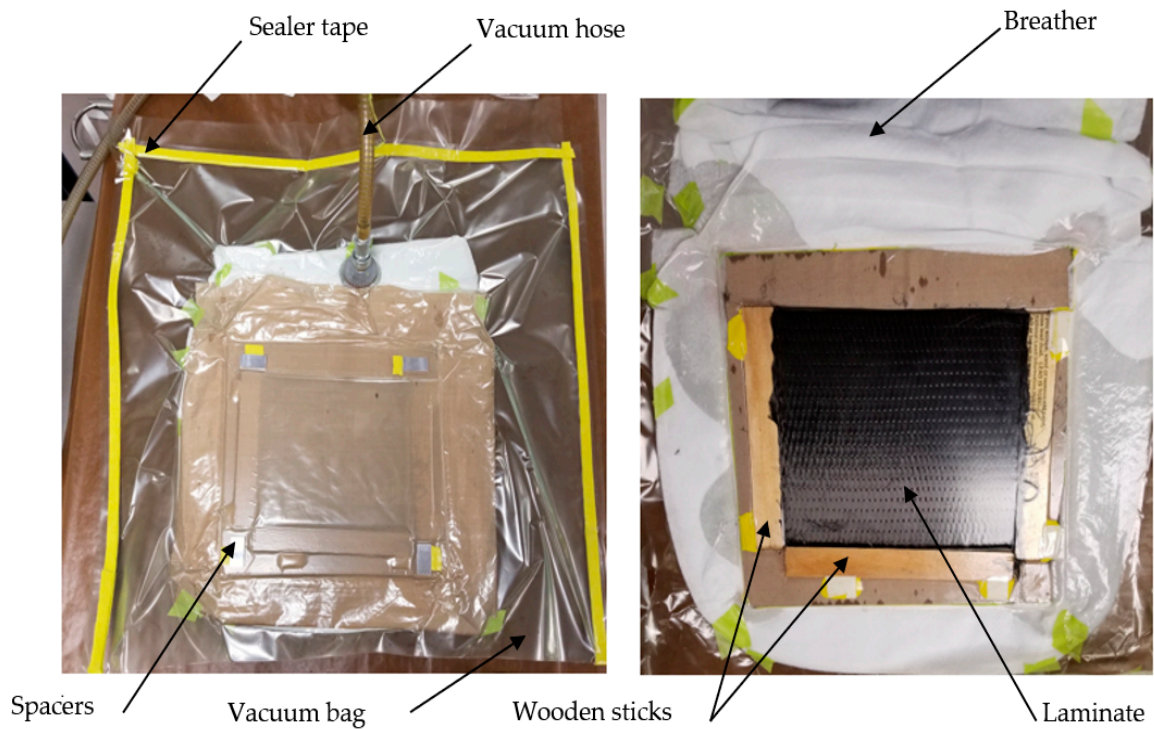


Figure 3. Contact molding assisted with vacuum bag and hot press.

Here, M_f is the surface density of the dry reinforcement (g/m^2); N is the number of plies; ϕ is the fiber density (g/m^3), and h is the laminate thickness (m).

Unlike the resin burn-off technique, this method does not reveal the emptiness ratio. Therefore, a porosity test was required. Micrographic image processing is deemed to be a good approach to evaluate the porosity level in laminates. Kite et al. [33] emphasized that the outcomes of this method correlate well with matrix digestion. Thus, 6 samples of each plaque were cut and prepared to be polished by a motopol 2000 automatic polisher. Next, an optical microscope was used to take a sufficient number of pictures of the whole sample's area with a magnification of 50X (Figure 4). Finally, an open-source software named ImageJ was used to segment this image into three zones: the background, the composite, and voids. This step was performed through machine learning, where the operator manually introduces all of these different sections to the software. Doing so, the software can determine the percentages of zones of the entire image.

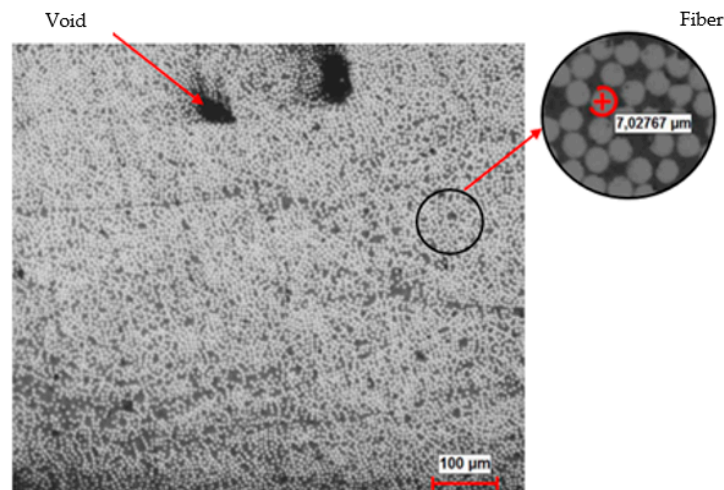


Figure 4. Microscopic picture X50.

2.3. Mechanical Test

The purpose of the short beam shear test is to investigate the matrix adhesion quality. This test is similar to the flexural test. However, the length of the short beam's coupon is short compared to the flexural coupon. Thus, the vertical force induces a shear stress in the plane of specimens. The ASTM D2344 standard requires precise geometrical and dimensional tolerances of the coupon. In order to respect these constraints, a high-precision cutting machine (Struers Secotom 50, Struers, Mississauga, ON, Canada) with a diamond saw was used. To guarantee representative results, ten coupons from each laminate with 0° fiber orientation were tested. The interlaminar shear strength (ILSS) tests were performed on a universal testing machine (MTS alliance RF/200, MTS systems corporation, Eden prairies, MN, USA) which was equipped with a 10 kN load cell. The crosshead speed was set at 1 mm/min and the interlaminar shear strength was calculated according to this equation.

$$\text{ILSS} = 0.75 \times (\text{Fmax}/A) \quad (6)$$

where ILSS is the interlaminar shear strength (N/mm²); Fmax is the maximum force (N), and A is the surface area of the coupon (mm²).

Ten flexural samples were prepared according to ASTM D7264. Like the short beam shear sample, the fiber orientation was kept at 0° and the crosshead speed of 1 mm/min was maintained until the first drop load occurred which indicates the breakage point. Based on the standard recommendations, the strain points of 0.001 and 0.003 were used to calculate the chord modulus of elasticity. Moreover, the ultimate flexural strength and chord modulus of elasticity were determined by implementing the maximum applied forces in Equations (7) and (8):

$$\sigma_f = (3 \times \text{Fmax} \times L)/(2 \times b \times h^2) \quad (7)$$

$$E_f = \Delta\sigma/\Delta\varepsilon \quad (8)$$

where Fmax is the maximum force (N); L is the specimen length (mm); h is the specimen thickness (mm); b is the specimen width (mm), and ε is the strain (mm/mm).

3. Results and Discussion

3.1. Fiber Volume Fraction

The developed manufacturing method induces repeatable results. Consistent fiber volume fraction is a must to distinguish between the effect of thickness variations and the effect of graphene particles. A digital micrometer was used to take four measurements of each laminate, and these values were then averaged and used in equation (5) to calculate the fiber volume fraction. The V_f mean value, between laminates, equals 64% ± 0.41%. This trivial variation can be ascribed to variation in the Teflon sheet thickness, the spacers thickness, and the mold surface flatness. Nonetheless, this variation is still acceptable, and its impact can be averted through a statistical normalization around the average value of V_f .

In the porosity analysis, the software ImageJ results in a "classifier" file, and this file is a template that contains data through which we can classify similar microscopic pictures. Subsequently, these pictures are converted into a binary image with black and white colors (Figure 5). White pixels with color under a certain threshold will be counted as voids; others with color above the threshold will be counted as composites. The software will then calculate the void percentage, which is the white area divided by the total area.



Figure 5. Binary microscopic image.

Figure 6 presents the void percentage of the composites versus the percentage of filler. As can be seen, the results are almost constant with a slight variation. The average value of porosity is equal to 0.61% with the smallest value of 0.4% and a maximum of 0.86%. The results are relatively good compared to the common standards. For instance, in aerospace applications, aircraft parts with a porosity level between 2.5% and 5% are usually accepted [34]. Nevertheless, Costa et al. [35] emphasized in their review that the interlaminar shear strength can be significantly affected if the porosity content goes beyond 0.9%. In addition, Hakim et al. [36] highlighted that higher porosity levels make the composite part sensitive to water penetration and environmental factors which detrimentally impact the static and fatigue strength. The minimum void percentage that we found can be attributed to the high vacuum pressure applied during the curing process. Hakim et al. [36] evaluated the impact of vacuum pressure on the porosity level. They examined three levels of vacuum pressure: poor (0 mmHg), medium (330 mmHg), and high (686 mmHg) and concluded that poor vacuum pressure induces 3.43% of porosity versus only 1.43% with high vacuum pressure. Furthermore, larger pores were more discernable with low vacuum pressure than with high vacuum pressure. According to the bar chart (Figure 6), the void percentage decreases as the filler percentages increase. For instance, laminates with 0 wt.% have 0.86% of void, whereas laminates with 3 wt.% have only 0.4% of void. Typically, increasing the load percentage would increase the matrix viscosity which hinders the extraction of the air bubbles and thus increases the porosity level. Consequently, the depicted pattern in the bar chart does not corroborate with the mentioned hypothesis. Indeed, this trend can be assigned to the detection accuracy of the software Image J. After a sheer number of iterations, the software gained the aptitude to identify various parts of the micrographic image with higher precision. Therefore, the depicted values of the void with 3 wt.% are calculated with relatively more accuracy than the ones of 0 wt.%. Nonetheless, all the presented values are less than 1% which is considered as the threshold for a good composite quality.

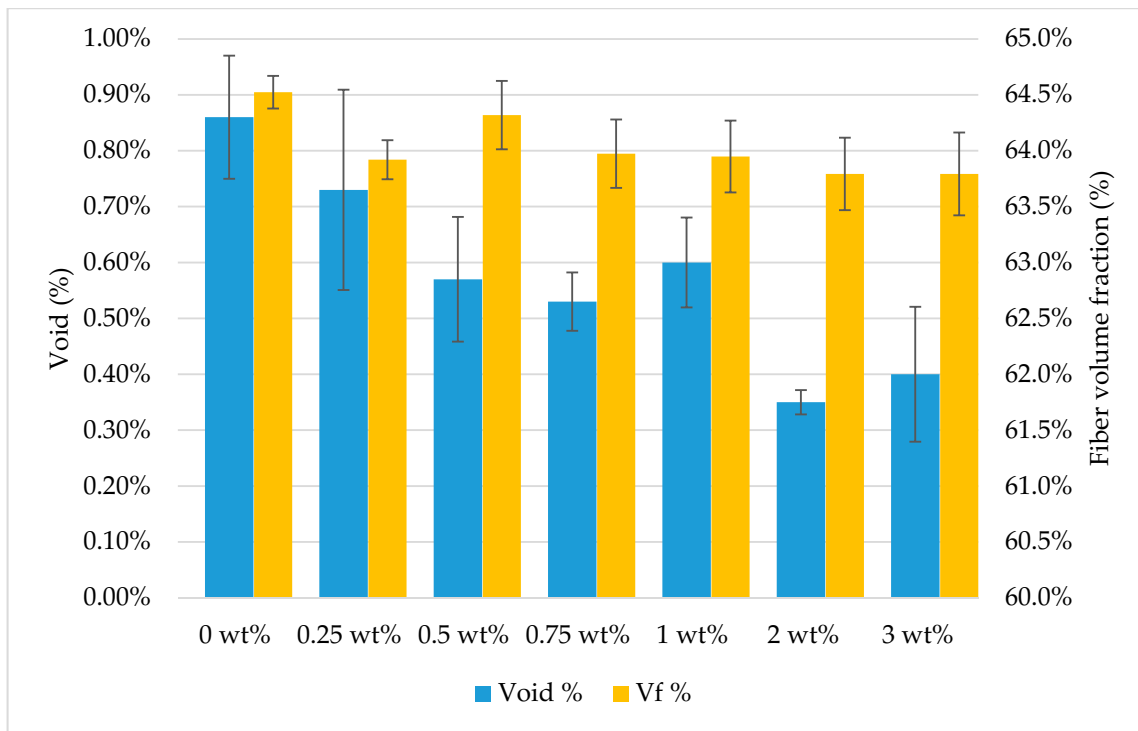


Figure 6. Fiber volume fraction and void of the composite.

3.2. Mechanical Test

A statistical study was required to detect and eliminate the outliers from the list of coupon results. These filtered results were then normalized using equation (9) to a $V_f = 64%$ [37].

$$\text{Normalized value} = (\text{test value} \times 0.64) / (\text{sample's } V_f) \tag{9}$$

A Pearson correlation test was performed on the normalized values versus the fiber volume fraction (V_f) variation. This test was done under a significance level of 5%. The null hypothesis states that there is no significant correlation between the mechanical properties outcomes versus the V_f variation. Most of the results did not reveal any significant correlation, therefore we can conclude that these results solely present the impact of the filler percentages. All flexural tests behaved linearly until the first drop of the load. This point was used to calculate the flexural strength for each sample. Figure 7 shows that the ultimate flexural strength of specimens with 0.25 wt.% improved by 5% compared to the pristine composite. It is important to mention that the fiber volume fraction of coupons with 0.25 wt.% is only 63.9% as opposed to 64.5% for plain coupons, which indicates that the 5% enhancement of flexural strength is purely assigned to the effect of the filler. On the other hand, the other laminates with a filler concentration higher than 0.25 wt.% demonstrated a slight decrease. The worst cases were with 2 and 3 wt.% with a drop of approximately 7% of the strength. A similar pattern was found by Kamar et al. [24], where they specified 1 wt.% as a threshold of the graphene percentage. Beyond this point, the filler particles start to agglomerate into relatively big bundles which weaken the interlaminar adhesion, thus leading to delamination and micro-buckling defects.

The stiffness of samples was calculated through Equation (8). Figure 7 presents the recorded results. No improvement was found by increasing the filler percentage. In contrast, the stiffness of the loaded specimens mildly decreased to a minimum of 125.7 GPa for the coupons with 0.5 wt.% as compared to a maximum of 131.4 GPa for the neat coupons. Both the stiffness and the ultimate shear strength of samples with 0.5 wt.% and higher filler contents are observed to decrease. This cannot be explained by the fiber volume fraction variation but rather by the effect of the graphene content, as can be seen by comparing the stiffness of samples with 0.25 wt.% and samples with 0.5 wt.% of

graphene content. The latter has a slightly higher fiber volume fraction and yet exhibits lower stiffness. In the case of the 0.25 wt.% concentration, the ultimate strength of this specimen showed a certain enhancement, but the stiffness is reduced. This does not meet the anticipated outcomes. For example, Hung et al. [38] investigated the impact of graphene oxide on the mechanical properties of CFRP, reporting an enhancement of around 18% and 5% in the flexural strength and the stiffness, respectively. Nonetheless, in the case of 0.25 wt.%, the Pearson correlation test demonstrated a vivid relation between the stiffness and the V_f variations (Figure 8). This was corroborated with previous studies [9,25], highlighting that flexural and tensile specimens with 0° fiber orientation are not sensitive to the matrix adhesion quality but rather to the fiber volume fraction and the fiber mechanical properties. Therefore, this trend can be assigned to the impact of V_f variation from one sample to another and not to the graphene percentage.

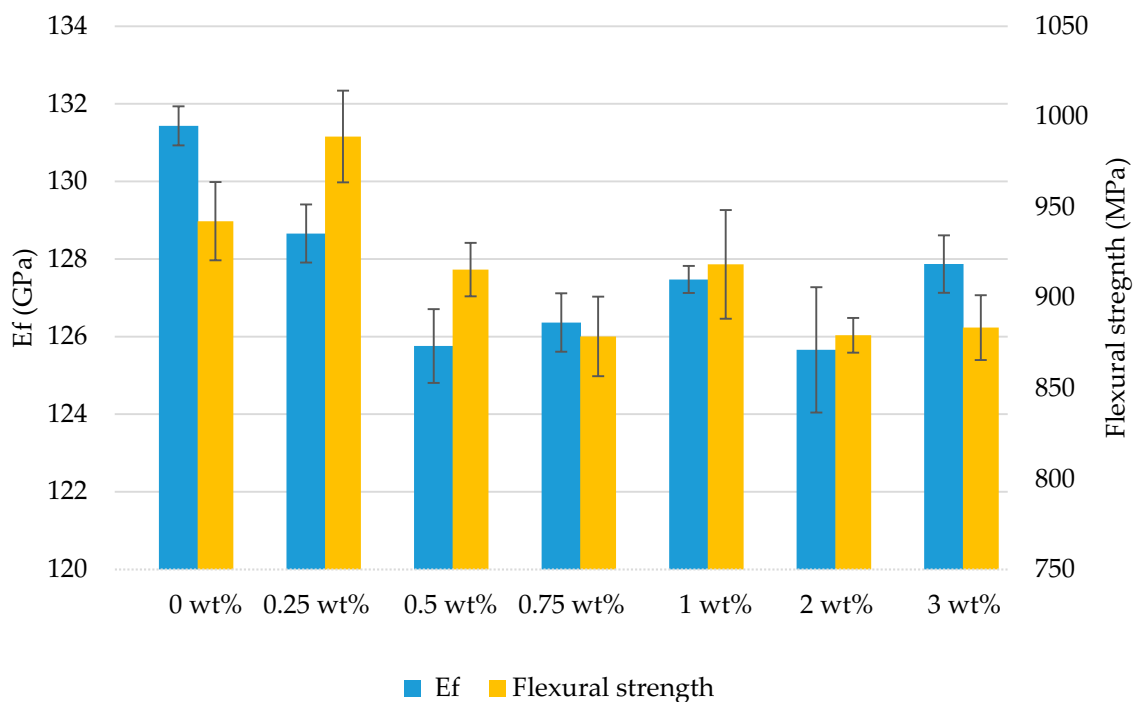


Figure 7. Stiffness and flexural strength of the composite.

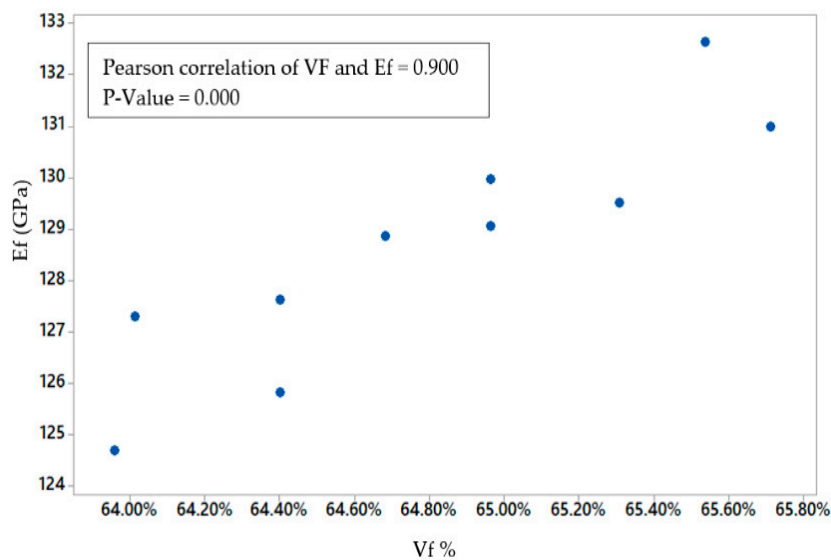


Figure 8. Scatter plot stiffness versus V_f variations of samples with 0.25 wt.%.

Figure 9 displays the mean values of the interlaminar shear strength (ILSS) of each filler percentage. Samples with 0.25 and 0.5 wt.% showed a decent increase ranging from 56 to approximately 59 MPa. The fiber content of the 0.25 wt.% coupons is less than the fiber content of plain coupons. Nonetheless, the recorded improvement counts as 5% in comparison to the neat composite. Meanwhile, 0.75 and 2 wt.% of graphene concentrations almost showed the same improvement of the ILSS by about 2%. However, the ILSS of all the specimens decreased with a minimum of 52 MPa in the case of 3 wt.%. The behavior of the ILSS largely depends on the graphene content, and in the case of low concentrations (0 to 0.5 wt.%), the ILSS behaves linearly with a positive slope. Beyond 0.75 wt.%, this linear relation appears to be inversely proportional, except for 2 wt.% which presents a certain enhancement. A similar trend was revealed by [23], though their tested graphene range was smaller, going from 0.1 to 0.4 wt.%. More experiments must be carried out to better understand this trend.

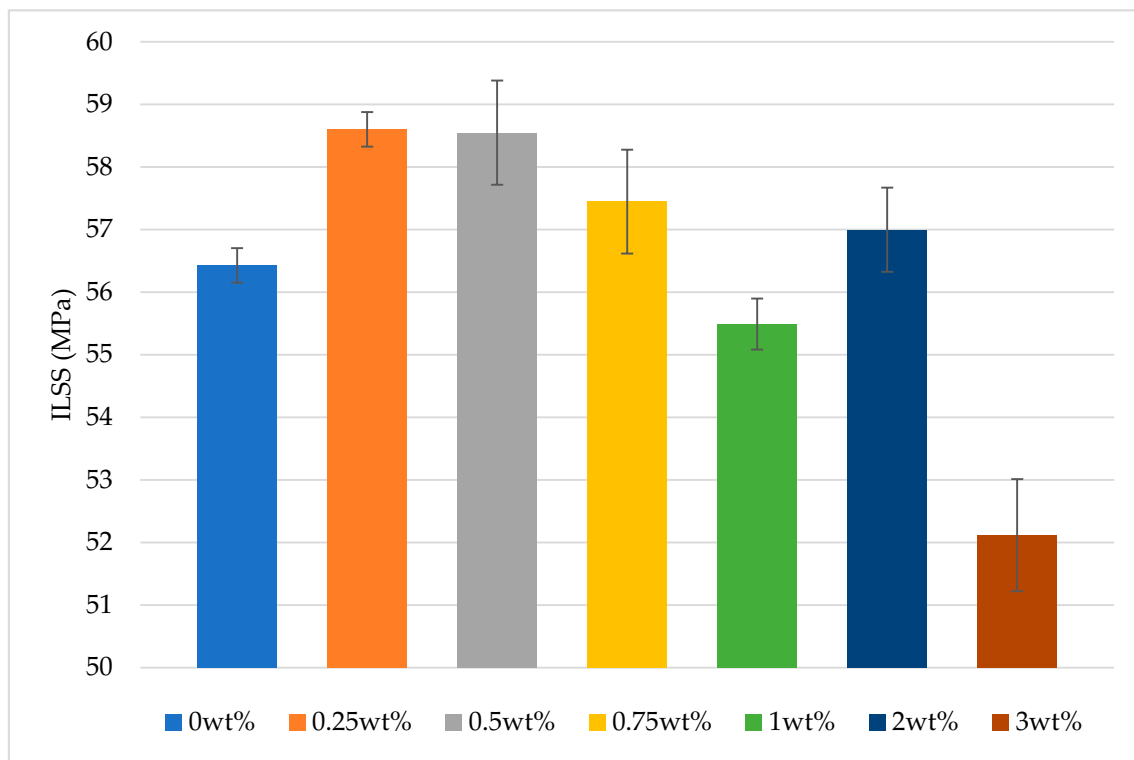


Figure 9. Interlaminar shear strength of the composites.

For further clarification, we have presented the relative details and figures of the previous diagrams in Table 3.

Table 3. Figures recapitulation.

GnPs wt.% %	V _f %	Void%	Flexural Strength (MPa)	Stiffness (GPa)	ILSS (MPa)
0	64.5	0.86	942.3	131.4	56.4
0.25	63.9	0.73	989.1	128.6	58.6
0.50	64.3	0.57	915.6	125.7	58.5
0.75	64.0	0.53	878.7	126.3	57.4
1.00	63.9	0.60	918.5	127.4	55.5
2.00	63.8	0.35	879.3	125.6	57
3.00	63.8	0.40	883.6	127.8	52.1

4. Conclusions

In this study, seven laminates of CFRP were manufactured by hand-layup assisted with vacuum bagging and hydraulic press, and these laminates contain different GnPs percentages ranging from 0 to 3 wt.%. The methodology process was described and has been approved as repeatable with low porosity and V_f variation. The manufactured laminates possess a consistent fiber volume fraction with an average value of 64%. The micrographic porosity test revealed an acceptable void content with a mean of 0.61%. Hence, the fiber volume fraction and the porosity level have little influence on the mechanical properties. Ten flexural samples and ten short beam samples were cut from each laminate, and this was performed according to the ASTM standards. The outcomes presented in this study lead to the following conclusion:

The best graphene percentage was 0.25 wt.%; samples with this filler content induced 5% improvement of the ILSS.

It appears that 0.5 wt.% presents a threshold of the graphene filler, so more than this value, the particles will coalesce which, in turn, results in a poor graphene dispersion and therefore the mechanical properties will be negatively affected.

The same trend was observed regarding the flexural test. Samples with 0.25 wt.% filler showed a maximum improvement of 5%. It was expected that the chord modulus of elasticity would reveal the same trend as the flexural strength. However, it seems that the stiffness is more prone to the fiber volume fraction content. Pearson correlation test showed that the stiffness and the V_f variation using this filler concentration are linearly proportional. Hence, it is difficult to conclude regarding this aspect.

For future studies, we should test other graphene percentages between 0 and 0.25 wt.%. Additionally, further tests should be carried on with 90° fiber orientation which might be more effective to evaluate the adhesion quality of the filled epoxy.

Author Contributions: J.-F.C., G.L. and C.O.-P. designed and directed the study. M.A.C. and R.M. developed the CFRP manufacturing method. M.A.C. performed all the experiments, measurements, and analysis of the results. The writing and revision of the manuscript were performed according to the order of the authors. All authors have read and agreed to the published version of the manuscript.

Funding: This work was co-funded by Nano-Xplore company and Natural Sciences and Engineering Research Council of Canada.

Acknowledgments: We would like to express our special gratitude to Giovanna Gutierrez, R&D Manager and Nima Moghimian, Director of R&D at Nano-Xplore for their technical support and the graphene particles supplied during this research. We also express our gratitude to Nabil Mazeghrane, and Éric Marcoux, from ETS, who provided technical assistance during the experiments.

Conflicts of Interest: The authors declare no conflict of interest.

References

1. Othman, R.; Ismail, N.I.; Basri, H.M.; Sharudin, H.; Hemdi, A.R. Application of carbon fiber reinforced plastics in automotive industry: A review. *J. Mech. Manuf.* **2018**, *1*, 12.
2. Zhang, J.Z. Study on Carbon Fiber Composite Materials in Sports Equipment. *Appl. Mech. Mater.* **2013**, *329*, 105–108. [[CrossRef](#)]
3. Breuer, U.P. *Commercial Aircraft Composite Technology*; Springer International Publishing: Cham, Switzerland, 2016.
4. Bouvet, C. *Mechanics of Aeronautical Composite Materials*; ISTE Ltd./John Wiley and Sons Inc.: Hoboken, NJ, USA, 2017; ISBN 978-1-78630-114-7.
5. Budynas, R.G.; Nisbett, J.K. *Shigley's Mechanical Engineering Design*, 9th ed.; McGraw-Hill: New York, NY, USA, 2011; ISBN 978-0-07-352928-8.
6. Shesan, O.J.; Stephen, A.C.; Chioma, A.G.; Neerish, R.; Rotimi, S.E. Fiber-Matrix Relationship for Composites Preparation. In *Renewable and Sustainable Composites*; Pereira, A.B., Fernandes, F.A.O., Eds.; IntechOpen: Rijeka, Croatia, 2019.

7. Liu, X.; Chen, F. A Review of Void Formation and its Effects on the Mechanical Performance of Carbon Fiber Reinforced Plastic. *Eng. Trans.* **2016**, *64*, 33–51.
8. Pathak, A.K.; Borah, M.; Gupta, A.; Yokozeki, T.; Dhakate, S. Improved mechanical properties of carbon fiber/graphene oxide-epoxy hybrid composites. *Compos. Sci. Technol.* **2016**, *135*, 28–38. [[CrossRef](#)]
9. Qin, W.; Vautard, F.; Drzal, L.T.; Yu, J. Mechanical and electrical properties of carbon fiber composites with incorporation of graphene nanoplatelets at the fiber–matrix interphase. *Compos. Part B Eng.* **2015**, *69*, 335–341. [[CrossRef](#)]
10. Novoselov, K.S.; Geim, A.K.; Morozov, S.V.; Jiang, D.; Zhang, Y.; Dubonos, S.V.; Grigorieva, I.V.; Firsov, A.A. Electric Field Effect in Atomically Thin Carbon Films. *Science* **2004**, *306*, 666–669. [[CrossRef](#)] [[PubMed](#)]
11. Kim, H.; Abdala, A.A.; Macosko, C.W. Graphene/Polymer Nanocomposites. *Macromolecules* **2010**, *43*, 6515–6530. [[CrossRef](#)]
12. Stankovich, S.; Dikin, D.A.; Dommett, G.H.B.; Kohlhaas, K.M.; Zimney, E.J.; Stach, E.A.; Piner, R.D.; Nguyen, S.T.; Ruoff, R.S. Graphene-based composite materials. *Nat. Cell Biol.* **2006**, *442*, 282–286. [[CrossRef](#)]
13. Balandin, A.A.; Ghosh, S.; Bao, W.; Calizo, I.; Teweldebrhan, D.; Miao, F.; Lau, C.N. Superior Thermal Conductivity of Single-Layer Graphene. *Nano Lett.* **2008**, *8*, 902–907. [[CrossRef](#)]
14. Lee, C.; Wei, X.; Kysar, J.W.; Hone, J. Measurement of the Elastic Properties and Intrinsic Strength of Monolayer Graphene. *Science* **2008**, *321*, 385–388. [[CrossRef](#)]
15. Yang, W.; Zhao, Q.; Xin, L.; Qiao, J.; Zou, J.; Shao, P.; Yu, Z.; Zhang, Q.; Wu, G. Microstructure and mechanical properties of graphene nanoplates reinforced pure Al matrix composites prepared by pressure infiltration method. *J. Alloys Compd.* **2018**, *732*, 748–758. [[CrossRef](#)]
16. Stoller, M.D.; Park, S.; Zhu, Y.; An, J.; Ruoff, R.S. Graphene-Based Ultracapacitors. *Nano Lett.* **2008**, *8*, 3498–3502. [[CrossRef](#)] [[PubMed](#)]
17. Nazarpour, S.; Waite, S.R. (Eds.) *Graphene Technology: From Laboratory to Fabrication*; Wiley-VCH Verlag GmbH & Co. KGaA: Weinheim, Germany, 2016.
18. Chen, G.-H.; Wu, D.-J.; Weng, W.-G.; Yan, W.-L. Preparation of polymer/graphite conducting nanocomposite by intercalation polymerization. *J. Appl. Polym. Sci.* **2001**, *82*, 2506–2513. [[CrossRef](#)]
19. Giannelis, E.P. Polymer Layered Silicate Nanocomposites. *Adv. Mater.* **1996**, *8*, 29–35. [[CrossRef](#)]
20. Sandler, J.; Pegel, S.; Cadek, M.; Gojny, F.; Van Es, M.; Lohmar, J.; Blau, W.; Schulte, K.; Windle, A.; Shaffer, M.S.P. A comparative study of melt spun polyamide-12 fibres reinforced with carbon nanotubes and nanofibres. *Polymer* **2004**, *45*, 2001–2015. [[CrossRef](#)]
21. Rafiee, M.A.; Rafiee, J.; Wang, Z.; Song, H.; Yu, Z.-Z.; Koratkar, N. Enhanced Mechanical Properties of Nanocomposites at Low Graphene Content. *ACS Nano* **2009**, *3*, 3884–3890. [[CrossRef](#)]
22. Al Imran, K. Enhancement of Electrical Conductivity of Carbon/Epoxy Composites by Graphene and Assessment of Thermal and Mechanical Properties. Ph.D. Thesis, North Carolina A&T State University, Greensboro, NC, USA, 2016.
23. Han, X.; Zhao, Y.; Sun, J.; Li, Y.; Zhang, J.; Hao, Y. Effect of graphene oxide addition on the interlaminar shear property of carbon fiber-reinforced epoxy composites. *New Carbon Mater.* **2017**, *32*, 48–55. [[CrossRef](#)]
24. Kamar, N.T.; Hossain, M.M.; Khomenko, A.; Haq, M.; Drzal, L.T.; Loos, A. Interlaminar reinforcement of glass fiber/epoxy composites with graphene nanoplatelets. *Compos. Part A Appl. Sci. Manuf.* **2015**, *70*, 82–92. [[CrossRef](#)]
25. Tang, L.-C.; Wan, Y.-J.; Yan, D.; Pei, Y.-B.; Zhao, L.; Li, Y.-B.; Wu, L.-B.; Jiang, J.-X.; Lai, G.-Q. The effect of graphene dispersion on the mechanical properties of graphene/epoxy composites. *Carbon* **2013**, *60*, 16–27. [[CrossRef](#)]
26. Raza, M.; Westwood, A.; Stirling, C. Effect of processing technique on the transport and mechanical properties of graphite nanoplatelet/rubbery epoxy composites for thermal interface applications. *Mater. Chem. Phys.* **2012**, *132*, 63–73. [[CrossRef](#)]
27. Chandrasekaran, S.; Seidel, C.; Schulte, K. Preparation and characterization of graphite nano-platelet (GNP)/epoxy nano-composite: Mechanical, electrical and thermal properties. *Eur. Polym. J.* **2013**, *49*, 3878–3888. [[CrossRef](#)]
28. McLaughlin, A.M. The Effect of Exfpmoated Graphite on Carbon Fiber Reinforced Composites for Cryogenic Applications. Ph.D. Thesis, University of Massachusetts Lowell, Ann Arbor, MA, USA, 2013.
29. Mayr, G.; Plank, B.; Sekelja, J.; Hendorfer, G. Active thermography as a quantitative method for non-destructive evaluation of porous carbon fiber reinforced polymers. *NDT E Int.* **2011**, *44*, 537–543. [[CrossRef](#)]

30. Chowdhury, F.; Hosur, M.; Jeelani, S. Studies on the flexural and thermomechanical properties of woven carbon/nanoclay-epoxy laminates. *Mater. Sci. Eng. A* **2006**, *421*, 298–306. [[CrossRef](#)]
31. El-Ghaoui, K.; Chatelain, J.F.; Ouellet-Plamondon, C.; Mathieu, R. Effects of Nano Organoclay and Wax on the Machining Temperature and Mechanical Properties of Carbon Fiber Reinforced Plastics (CFRP). *J. Compos. Sci.* **2019**, *3*, 85. [[CrossRef](#)]
32. Mehdikhani, M.; Gorbatiikh, L.; Verpoest, I.; Lomov, S.V. Voids in fiber-reinforced polymer composites: A review on their formation, characteristics, and effects on mechanical performance. *J. Compos. Mater.* **2018**, *53*, 1579–1669. [[CrossRef](#)]
33. Kite, A.H.; Hsu, D.K.; Barnard, D.J.; Thompson, D.O.; Chimenti, D.E. Determination of Porosity Content in Composites by Micrograph Image Processing. In *AIP Conference Proceedings*; American Institute of Physics: Golden, CO, USA, 2008; Volume 975, pp. 942–949. [[CrossRef](#)]
34. Kastner, J.; Plank, B.; Salaberger, D.; Sekelja, J. Defect and Porosity Determination of Fibre Reinforced Polymers by X-ray Computed Tomography. In *Proceedings of the 2nd International Symposium on NDT in Aerospace*, Hamburg, Germany, 22–24 November 2010; pp. 1–12.
35. Costa, M.L.; Almeida, S.F.M.; Rezende, M.C. The influence of porosity on the interlaminar shear strength of carbon/epoxy and carbon/bismaleimide fabric laminates. *Compos. Sci. Technol.* **2001**, *61*, 2101–2108. [[CrossRef](#)]
36. Hakim, I.; Donaldson, S.L.; Meyendorf, N.; Browning, C. Porosity Effects on Interlaminar Fracture Behavior in Carbon Fiber-Reinforced Polymer Composites. *Mater. Sci. Appl.* **2017**, *8*, 170–187. [[CrossRef](#)]
37. Technomic Publishing Company (Ed.) *The Composite Materials Handbook: MIL 17, Volume 3: Materials, Usage, Design, and Analysis*; Technomic Publ.: Lancaster, UK, 1999.
38. Hung, P.-Y.; Lau, K.-T.; Qiao, K.; Fox, B.; Hameed, N. Property enhancement of CFRP composites with different graphene oxide employment methods at a cryogenic temperature. *Compos. Part A Appl. Sci. Manuf.* **2019**, *120*, 56–63. [[CrossRef](#)]

Publisher's Note: MDPI stays neutral with regard to jurisdictional claims in published maps and institutional affiliations.



© 2020 by the authors. Licensee MDPI, Basel, Switzerland. This article is an open access article distributed under the terms and conditions of the Creative Commons Attribution (CC BY) license (<http://creativecommons.org/licenses/by/4.0/>).